Estimating interdependences in networks of weakly coupled deterministic systems

Oscar De Feo*
Department of Microelectronic Engineering, University College Cork, North Mall, Cork, Ireland

Cristian Carmeli†
Laboratory of Nonlinear Systems, Swiss Federal Institute of Technology Lausanne, EPFL IC LANOS, Station 14, 1015 Lausanne, Switzerland

(Received 15 May 2006; revised manuscript received 20 December 2007; published 27 February 2008)

The extraction of information from measured data about the interactions taking place in a network of systems is a key topic in modern applied sciences. This topic has been traditionally addressed by considering bivariate time series, providing methods which are sometimes difficult to extend to multivariate data, the limiting factor being the computational complexity. Here, we present a computationally viable method based on black-box modeling which, while theoretically applicable only when a deterministic hypothesis about the processes behind the recordings is plausible, proves to work also when this assumption is severely affected. Conceptually, the method is very simple and is composed of three independent steps: in the first step a state-space reconstruction is performed separately on each measured signal; in the second step, a local model, i.e., a nonlinear dynamical system, is fitted separately on each (reconstructed) measured signal; afterward, a linear model of the dynamical interactions is obtained by cross-relating the (reconstructed) measured variables to the dynamics unexplained by the local models. The method is successfully validated on numerically generated data. An assessment of its sensitivity to data length and modeling and measurement noise intensity, and of its applicability to large-scale systems, is also provided.

DOI: 10.1103/PhysRevE.77.026711 PACS number(s): 05.10.−a

I. INTRODUCTION

A key topic in modern applied sciences is the process of unraveling the principles governing the functional interactions within a network of coupled dynamical systems [1–5]. For instance, in population biology the interest is focused on interactions between different populations in a given territory [6], while in neuroscience a key question is how single neurons process a certain stimulus within functionally coherent neuronal assemblies [7].

The process of inferring the functional topology of such networks is crucial to understanding the mechanisms of interaction, eventually leading to the formulation of a prediction of their dynamical behavior [8,9]. Usually, this process consists of estimating the strength and direction of the interdependences among measured signals (time series). Traditionally, this estimation has been done by methods assessing the synchrony among the observed dynamical systems [10–12]. However, this approach is limiting because it does not estimate coupling directionality, which is important, for example, to unravel driver-response interdependences [13]. For this reason, many methods have been proposed recently to address this issue: some of them take inspiration from information theory [12,14] and others exploit salient properties of deterministic systems such as predictability [13,15,16] or phase dynamics [17,18]. Unfortunately, most of these methods have been introduced for dealing with bivariate time series and can lead to misleading interpretations when applied to multivariate data, because they are not able to discriminate between indirect and direct relationships [19].

The need for multivariate analysis has increased recently with the growing availability of multiple parallel measurements in modern experimental setups. For stochastic processes, this multivariate analysis has already been applied successfully [20–23]. For deterministic processes, we can consider two cases: weakly and strongly interacting dynamical systems. In the latter case, strong couplings are seen as inducing phenomena of synchrony, and methods are already available for their estimation [24,25]. In the former case, the estimation of weak couplings has been approached in [26] by using a nonlinear Granger causality index, in [27,28] by considering the phase dynamics, and in [29] by using conditional mutual information, an established tool of information theory [30]. Furthermore, some methods have been proposed within a particular application in neuroscience [31,32].

Here, we address the problem of estimating the strength and direction of weak interdependences between multivariate time series when a deterministic hypothesis about the processes behind the recordings is plausible. The proposed approach is similar to the one proposed in [27], though here the whole dynamics, and not only the phase dynamics, are considered. More precisely, the approach consists of building a functional model from the multivariate data by identifying an autonomous multioutput system. However, such a "black-box" modeling approach may quickly become computationally intractable, and simplifying assumptions have to be made. For the case of weakly interacting dynamical systems, we proceed as follows. For each measured signal, we reconstruct separately a nonlinear dynamical system. Then, by assuming weak (linear) interactions, we construct a linear

*oscar.defeo@ucc.ie
†Present address: Department of Electronics & Information Engineering, Hong Kong Polytechnic University, Hung Hom Kowloon, Hong Kong. cristian.carmeli@polyu.edu.hk

model of the interactions by means of a classical linear multioutput system identification method.

A detailed description of the method is given in Sec. II, while in Sec. III we test numerically the ability of the method to correctly estimate couplings within networks of two and three dynamical systems. In Sec. IV, we illustrate its sensitivity with respect to the length of data sets and measurement and modeling noise intensity, and its performance is compared with a reference method. In Sec. V, we discuss its applicability to large-scale systems. Finally, a discussion and conclusions are given in Sec. VI.

II. METHOD

Here, we illustrate a method to estimate the connectivity matrix of several interacting dynamical systems by assuming that such a network is composed of weakly coupled heterogeneous dynamical subsystems.

We denote by $\Theta(t) \in \mathbb{R}^D$, where

$$\Theta(t) = \begin{bmatrix} \theta^{(1)}(t) \\ \vdots \\ \theta^{(i)}(t) \\ \vdots \\ \theta^{(M)}(t) \end{bmatrix},$$

the state-space vector at time t of the M dynamical subsystems. The components $\theta^{(i)}(t) \in \mathbb{R}^{d^{(i)}}$ are the state variables of the generic $d^{(i)}$-dimensional subsystems (i) and $\Sigma_{i=1}^{M} d^{(i)} = D$. The network model is given by the noise-driven system

$$\dot{\Theta}(t) = \mathcal{F}(\Theta(t)) + \eta(t), \tag{1}$$

where the vector field $\mathcal{F}: \mathbb{R}^D \to \mathbb{R}^D$ is assumed continuous and differentiable. The vector $\eta(t) \in \mathbb{R}^D$ represents the unavoidable modeling noise, which we assume to be a zero-mean Gaussian additive process with covariance function $\langle \eta(t), \eta(t') \rangle = R\delta(t-t')$ and diagonal covariance matrix R, which is independent of $\mathcal{F}(\Theta(t))$ and has low intensity compared to that of $\mathcal{F}(\Theta(t))$, such that the hypothesis of determinism of the network dynamics is still tenable.

Let us focus on a generic subsystem (i). Under the hypothesis of *weak coupling*, the equation governing the (i)th dynamics can be written as

$$\dot{\theta}^{(i)}(t) = \mathcal{F}_S^{(i)}(\theta^{(i)}(t)) + \varepsilon \mathcal{F}_C^{(i)}(\Theta(t)) + \eta^{(i)}(t), \tag{2}$$

where $\mathcal{F}_S^{(i)}: \mathbb{R}^{d^{(i)}} \to \mathbb{R}^{d^{(i)}}$ describes the self-dynamics of the subsystem (i) in the absence of interactions within the network; $\mathcal{F}_C^{(i)}: \mathbb{R}^D \to \mathbb{R}^{d^{(i)}}$, weighted by the small constant ε, describes the weak intersubsystem interactions (couplings); and $\eta^{(i)} \in \mathbb{R}^{d^{(i)}}$ is the (i)th subvector of η.

Under the assumption of Eq. (2), the average interdependences along a given trajectory $\tilde{\Theta}(t)$ between the subsystem (i) and any other subsystem (j) can be naturally quantified as

$$\mathcal{K}^{(i,j)} = \frac{1}{T} \int_0^T \left. \varepsilon \frac{\partial \mathcal{F}_C^{(i)}}{\partial \theta^j} \right|_{\Theta = \tilde{\Theta}(\xi)} d\xi, \quad \forall \quad j \neq i, \tag{3}$$

where T is the time horizon of the trajectory $\tilde{\Theta}(t)$. Afterward, by means of a suitable arrangement of all the $\mathcal{K}^{(i,j)}$, $i,j = 1, \ldots, M$, the matrix $\mathcal{K}$ describing the connectivity within the network can be given as

$$\mathcal{K} = \begin{bmatrix} \emptyset & \cdots & \mathcal{K}^{(1,i)} & \cdots & \mathcal{K}^{(1,j)} & \cdots & \mathcal{K}^{(1,M)} \\ \vdots & \ddots & \vdots & & \vdots & & \vdots \\ \mathcal{K}^{(i,1)} & \cdots & \emptyset & \cdots & \mathcal{K}^{(i,j)} & \cdots & \mathcal{K}^{(i,M)} \\ \vdots & & \vdots & \ddots & \vdots & & \vdots \\ \mathcal{K}^{(j,1)} & \cdots & \mathcal{K}^{(j,i)} & \cdots & \emptyset & \cdots & \mathcal{K}^{(j,M)} \\ \vdots & & \vdots & & \vdots & \ddots & \vdots \\ \mathcal{K}^{(M,1)} & \cdots & \mathcal{K}^{(M,i)} & \cdots & \mathcal{K}^{(M,j)} & \cdots & \emptyset \end{bmatrix},$$

where the generic submatrix $\mathcal{K}^{(i,j)}$ of dimension $d^{(i)} \times d^{(j)}$ models the coupling from the subsystem (j) to the subsystem (i), and the diagonal blocks, representing the self-couplings, are by assumption set to zero and consequently denoted by $\emptyset$.

The goal is to estimate $\mathcal{K}$ from measurements. This task is not straightforward because we do not have normally a direct access to the state $\Theta(t)$; however, an observable of it, $Y(t)$, is usually available. Here, covering a wide range of situations, $Y(t)$ is assumed to be related to $\Theta(t)$ by a measurement function $\mathcal{G}: \mathbb{R}^D \to \mathbb{R}^P$, which we assume to be smooth and corrupted by some measurement noise $\nu(t)$, which is additive, zero mean, Gaussian distributed, and independent of $\mathcal{G}(\Theta(t))$.

Moreover, accounting for the fact that measurements are usually performed with a fixed uniform sampling interval δt at times $t_0, t_0 + \delta t, \ldots, t_0 + (L-1)\delta t$, and by denoting discrete time values as subscripts, we write the measurement equation of the network as

$$Y_t = \mathcal{G}(\Theta_t) + \nu_t, \tag{4}$$

yielding a P-variate time series Y_t, where $t = 0, \ldots, L-1$, and $\delta t = 1$, without loss of generality.

Let us now further assume that we have available $P = M$ measurements. Denoting by $y_t^{(i)}$, $t = 0, \ldots, L-1$, the (i)th scalar time series, we further assume the (i)th component of Eq. (4) to be a function of $\theta^{(i)}$ only, namely,

$$y_t^{(i)} = \mathcal{G}^{(i)}(\theta_t^{(i)}) + \nu_t^{(i)}. \tag{5}$$

In other words, we exclude the case where one or several subsystems are not observed and, if more than one observable is measured from the same subsystem, we assume that a preprocessing technique has been applied to coalesce them into one.

Under these assumptions, we may proceed to the estimation of the influences model $\mathcal{K}$ in three steps: Step 1, a series of state-space reconstructions, i.e., a state-space reconstruction is performed separately on each measured signal; step 2, a series of nonlinear regressions, i.e., a nonlinear dynamical system is fitted separately on each (reconstructed) measured signal; and step 3, a linear regression, i.e., a regression be-

tween all the (reconstructed) measured variables and the dynamics unexplained by the local models obtained at the previous step.

Before going into further details, it should be noted that each one of these steps relies on standard techniques, i.e., state-space reconstruction and (non)linear regressions; hence, they can be implemented in many ways. In the following, we will propose a specific implementation for them; however this is not meant to be a universal solution but, better still, an good one on average, resulting as the trade-off between robustness and computational cost under completely blind assumptions. In fact, we would like to stress that the key point of the approach is the decomposition into these three steps; the specific algorithmic implementation of each one of them can and should be tuned to the particular case at hand, exploiting in this way every piece of *a priori* knowledge.

Finally, to help the reader, we emphasize that, in this section, subscripts denote discrete values, like sampling time, while superscripts refer to subsystems.

A. First step: State-space reconstruction

The method exploits dynamical state-space properties of the data; hence, the first step is to reconstruct a state space that is topologically equivalent to the original one [33]. Because of the weak interactions, by embedding the time series $y^{(i)}$ of Eq. (5) we can expect to obtain a state space $x^{(i)} \in \mathbb{R}^{n^{(i)}}$ that is dynamically equivalent to the original $\theta^{(i)}$ and not to the whole Θ. This is done on all M measurements, getting the *mixed state space* $X \in \mathbb{R}^N$ of the network,[1] where $N = \sum_{i=1}^{M} n^{(i)}$.

B. Second step: Self-modeling

By following the assumption in Sec. II A and naturally moving to discrete time equations, we use Eq. (2) to write the dynamics of the reconstructed subsystem (i) as

$$x_{t+1}^{(i)} = F_S^{(i)}(x_t^{(i)}) + \varepsilon F_C^{(i)}(X_t) + \xi_t^{(i)}, \tag{6}$$

where, again, the function $F_S^{(i)}: \mathbb{R}^{n^{(i)}} \to \mathbb{R}^{n^{(i)}}$ describes the dynamics of the subsystem (i) in the absence of interactions, i.e., the (i)th subsystem "self-dynamics;" $F_C^{(i)}: \mathbb{R}^N \to \mathbb{R}^{n^{(i)}}$, weighted by the small constant ε, describes the weak inter-subsystem interactions (couplings), and $\xi_t^{(i)} \in \mathbb{R}^{n^{(i)}}$ accounts for the modeling noise.

Let us consider a generic reconstructed trajectory $\tilde{X}_t$, and let us assume, without loss of generality, that it has zero mean and that $F_C^{(i)}(0) = 0$. Then, by Taylor expansion (up to the first order) about the average point of the trajectory (the origin) of the second term of Eq. (6), we obtain

$$x_{t+1}^{(i)} = F_S^{(i)}(x_t^{(i)}) + \sum_{j \neq i} \varepsilon \frac{\partial F_C^{(i)}(X)}{\partial x^{(j)}}\bigg|_{X=0} x_t^{(j)} + \varepsilon \mathcal{O}(\|X_t\|^2) + \xi_t^{(i)}, \tag{7}$$

where the $n^{(i)} \times n^{(j)}$ matrices $\varepsilon \frac{\partial F^{(i)}}{\partial x^{(j)}}|_{X=0}$ describe the average couplings directed from the $n^{(j)}$ state variables of subsystem (j) to the $n^{(i)}$ state variables of subsystem (i).

According to the hypothesis of weak interactions within the network, the term $\omega_t^{(i)} = \sum_{j \neq i} \varepsilon \frac{\partial F_C^{(i)}(X)}{\partial x^{(j)}}|_{X=0} x_t^{(j)} + \varepsilon \mathcal{O}(\|X_t\|^2) + \xi_t^{(i)}$ on the right-hand side of Eq. (7) can be considered small with respect to the self-dynamic $F_S^{(i)}(x_t^{(i)})$. Hence, given

$$x_{t+1}^{(i)} = F_S^{(i)}(x_t^{(i)}) + \omega_t^{(i)}, \tag{8}$$

where $\omega_t^{(i)}$ is considered as a small modeling noise, and neglecting its small dependence on $F_S^{(i)}(x_t^{(i)})$, we proceed to identify $F_S^{(i)}$ from the pairs $(x_{t+1}^{(i)}, x_t^{(i)})$. In particular, in the absence of any further hypothesis that may help in better tuning the regression, we propose to use a least-squares (in predictive sense) algorithm. That is, for each subsystem (i), we estimate a model $\hat{F}_S^{(i)}$ from data so as to minimize the total square prediction error, i.e.,

$$\hat{F}_S^{(i)} = \arg \min_{F_S^{(i)}} \sum_{k=1}^{l^{(i)}-1} \|x_k^{(i)} - F_S^{(i)}(x_{k-1}^{(i)})\|^2,$$

where $\|\cdot\|$ stands for the two-norm and $l^{(i)}$ is the number of samples available for subsystem (i) after the embedding.

C. Third step: Cross modeling

Using the self-model $\hat{F}_S^{(i)}$ estimated at the previous step, we can introduce the modeling residuals $r^{(i)}$, i.e.,

$$r_t^{(i)} = x_t^{(i)} - \hat{x}_t^{(i)}, \tag{9}$$

where $\hat{x}_t^{(i)} = \hat{F}_S^{(i)}(x_{t-1}^{(i)})$ is the current state predicted on the basis of the only local past information $x_{t-1}^{(i)}$. These residuals represent the dynamics unjustified by the estimated local self-models. As a next step, we justify these residual dynamics with the dynamical interactions within the network. In practice, according to Eq. (7) we can rewrite Eq. (9) as

$$r_{t+1}^{(i)} = \sum_{j \neq i} \varepsilon \frac{\partial F_C^{(i)}(X)}{\partial x^{(j)}}\bigg|_{X=0} x_t^{(j)} + \epsilon_t^{(i)}, \tag{10}$$

where $\epsilon_t^{(i)}$ accounts for the higher-order terms of Eq. (7) and the modeling noise; hence, it is small under the hypothesis of deterministic dynamics and weak interactions, and with a small dependence on X_t, which we neglect. By exploiting the linearity of Eq. (10), the $(n^{(i)} \times \sum_{j \neq i} n^{(j)})$ coupling matrices $\hat{K}^{(i,j)} = \varepsilon \frac{\partial F_C^{(i)}(X)}{\partial x^{(j)}}|_{X=0}$ can be estimated via a linear regression between the tuples $(r_{t+1}^{(i)}, x_t^{(j)})_{\forall\ j \neq i}$. Once again, in the absence of any further hypothesis that may help in better tuning the linear regression, we propose to use a least-squares (in the predictive sense) algorithm. In particular, for each subsystem (i), we estimate the $\hat{A}^{(i)}$ $(n^{(i)} \times \sum_{j \neq i} n^{(j)})$ matrix as

$$\hat{A}^{(i)} = \arg \min_{A^{(i)}} \sum_{k=1}^{\min\{l^{(i)}\}-1} \|r_k^{(i)} - A^{(i)} X_{k-1}^{(\neg i)}\|^2,$$

where $X^{(\neg i)}$ is the state vector without the (i)th subsystem components. Consequently, the estimated matrix

[1] Mixed state space is a term that was formally introduced in [15].

$$\hat{A}^{(i)} = [\hat{K}^{(i,1)} \cdots \hat{K}^{(i,j\neq i)} \cdots \hat{K}^{(i,M)}]$$

is the concatenation of all the nonzero coupling matrices. Clearly, the estimate of the whole network connectivity matrix $\hat{K}$ follows straightforwardly as a suitable rearrangement of the estimated sub-blocks

$$\hat{K} = \begin{bmatrix} \emptyset & \cdots & \hat{K}^{(1,i)} & \cdots & \hat{K}^{(1,j)} & \cdots & \hat{K}^{(1,M)} \\ \vdots & \ddots & \vdots & & \vdots & & \vdots \\ \hat{K}^{(i,1)} & \cdots & \emptyset & \cdots & \hat{K}^{(i,j)} & \cdots & \hat{K}^{(i,M)} \\ \vdots & & \vdots & \ddots & \vdots & & \vdots \\ \hat{K}^{(j,1)} & \cdots & \hat{K}^{(j,i)} & \cdots & \emptyset & \cdots & \hat{K}^{(j,M)} \\ \vdots & & \vdots & & \vdots & \ddots & \vdots \\ \hat{K}^{(M,1)} & \cdots & \hat{K}^{(M,i)} & \cdots & \hat{K}^{(M,j)} & \cdots & \emptyset \end{bmatrix}.$$

D. Remarks

In a generic framework, the use of least-squares procedures is justified by the fact that, under our deterministic and weak-coupling hypotheses, we want to minimize the random disturbances $\omega_t^{(i)}$ in Eq. (8), and $\epsilon_t^{(i)}$ in Eq. (10). In particular, concerning the second (linear) least-squares procedure, it is important to notice two facts. First, the coupling estimated via this procedure is the average coupling with respect to the average point of the trajectory (center of the expansion). In general, this does not coincide with the ideal estimate of the coupling, i.e., the average value of the instantaneous couplings as given by Eq. (3), although this latter generally cannot be inferred in a completely blind setup like the one considered here. Second, if ordinary least-squares procedures are considered, the estimated couplings will be unbiased under the assumption that the additive noises, i.e., the $\epsilon_t^{(i)}$ in Eq. (10), have zero means and equal variances, and are mutually uncorrelated. In general, these hypotheses will never hold in the applications, in addition because the $\epsilon_t^{(i)}$ account for the modeling noise which surely introduces some correlation. However, if necessary, it is easy to consider a heteroscedasticity-consistent least-squares estimator to account for the heteroscedasticity and correlation of the noises [34]; though which kind of estimator to use will depend heavily on the hypotheses and application considered. Hereafter (cf. Sec. III), in the absence of further hypotheses, to keep the method simple we have only accounted for the heteroscedasticity of the noises but not for their correlations.

As a further advantage, the ordinary least-squares estimation also supplies a formula for computing the covariance matrix of the estimates. This further allows us to compute statistical hypotheses tests concerning the estimated coupling matrices $\hat{K}^{(i,j)}$ [34], which will allow a rigorous statistical analysis in Sec. III B. However, it is important to notice that the statistical analysis proposed (cf. Appendix A) relies on F tests [34]; hence, it implicitly assumes that the noises and errors are normally distributed. To what extent this hypothesis can be considered satisfied depends on the specific application, and if it is severely violated, nonparametric testing should be considered instead of F tests [35].

In conclusion, it should be noted that usually a single number quantifying the influence from $y^{(j)}$ to $y^{(i)}$ is more suitable than a matrix. Therefore, we propose to compute a norm of $\hat{K}^{(i,j)}$. For instance, the one-norm would correspond to detecting the strongest influence under the assumption that each $y^{(i)}$ is a linear observation of the corresponding $x^{(i)}$.

III. METHOD VALIDATION

In this section we test the ability of the method to estimate correctly couplings among interacting systems under the hypotheses described in Sec. II. In particular, we address two issues: first, the assessment of the directionality of the coupling in the case of two mutually coupled systems; second, the ability to discern between direct and indirect couplings among three interacting systems.

A. Numerical setup

In the first numerical example, we considered two nonidentical Lorenz dynamical systems [36], coupled as in Fig. 1(a). The corresponding dynamical equations are

$$\begin{aligned} \dot{\theta}_1^{(1)} &= \sigma^{(1)}(\theta_2^{(1)} - \theta_1^{(1)}) + \eta_1^{(1)}, \\ \dot{\theta}_2^{(1)} &= r^{(1)}\theta_1^{(1)} - \theta_2^{(1)} - \theta_1^{(1)}\theta_3^{(1)} + \mathcal{C}^{(1,2)}(\theta_2^{(1)} - \theta_2^{(2)}) + \eta_2^{(1)}, \\ \dot{\theta}_3^{(1)} &= \theta_1^{(1)}\theta_2^{(1)} - \beta^{(1)}\theta_3^{(1)} + \eta_3^{(1)}, \\ \dot{\theta}_1^{(2)} &= \sigma^{(2)}(\theta_2^{(2)} - \theta_1^{(2)}) + \eta_1^{(2)}, \\ \dot{\theta}_2^{(2)} &= r^{(2)}\theta_1^{(2)} - \theta_2^{(2)} - \theta_1^{(2)}\theta_3^{(2)} + \mathcal{C}^{(2,1)}(\theta_2^{(1)} - \theta_2^{(2)}) + \eta_2^{(2)}, \\ \dot{\theta}_3^{(2)} &= \theta_1^{(2)}\theta_2^{(2)} - \beta^{(2)}\theta_3^{(2)} + \eta_3^{(2)}, \end{aligned} \tag{11}$$

where $\theta_j^{(1)}, \theta_j^{(2)}$, $j=1,2,3$, are the state variables of the first and second oscillators, respectively; $\sigma^{(i)}$, $r^{(i)}$, and $\beta^{(i)}$, $i=1,2$, are parameters whose values are chosen randomly in a small interval ($\pm 5\%$) around the standard values 10, 27, and 8/3, respectively; $\eta_j^{(i)}$, $i=1,2$, $j=1,2,3$, are zero-mean uncorrelated Gaussian random noises (set in simulations to a variance of 1% of the energy of the right-hand side along the uncoupled attractors); and $\mathcal{C}^{(1,2)}$ and $\mathcal{C}^{(2,1)}$ are the strengths of diffusive couplings between the second-state variables $\theta_2^{(1)}$ and $\theta_2^{(2)}$. Their values are varied within the interval [0,0.5], which guarantees the validity of the hypothesis of weakly interacting oscillators. In particular, this interval was chosen such that the synchronization measure introduced in [25], which can take values ranging from 0 (for uncoupled subsystems) up to 1 (for perfectly synchronized subsystems), was lower than 0.15 almost everywhere.

For every considered value of the couplings $\mathcal{C}^{(1,2)}$ and $\mathcal{C}^{(2,1)}$, the differential equations were iterated, starting from random initial conditions, using the Heun algorithm [37] with $\delta t = 0.005$, which was checked to yield numerically stable results. In order to eliminate transients, the first 10 000 iterations were discarded. Then, after performing a down-

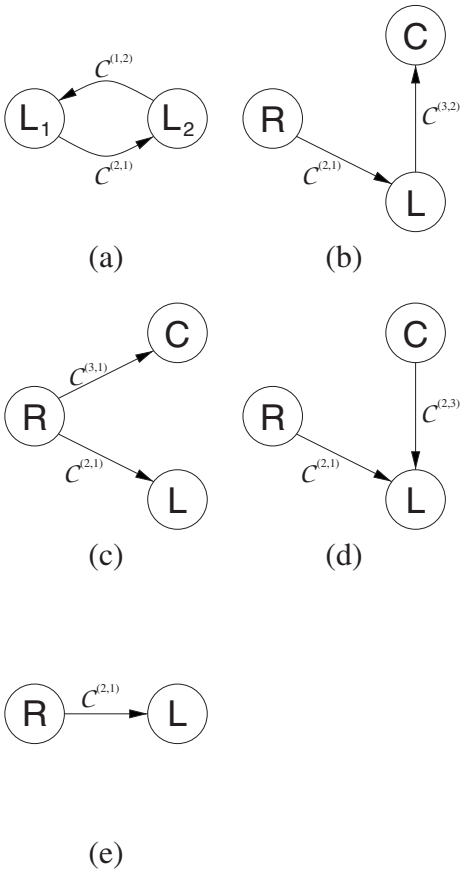

FIG. 1. Connection setups used for the validation of the method. (a) Setup for the directionality assessment—two Lorenz (L_1 and L_2) dynamical systems mutually coupled, cf. Eq. (11). (b)–(d) Setups for triangular interdependence assessments—coupled Rössler (R), Lorenz (L), and Colpitts (C) dynamical systems, cf. Eq. (12). Cases of (b) chain connection, (c) common source, and (d) common child. (e) Setup for the robustness assessment; nonlinearly coupled Rössler (R) and Lorenz (L) dynamical systems [cf. Eq. (13)].

sampling operation[2] at $\delta T=0.02$, time series of lengths $L=500$ were collected. To ensure repeatability and statistical stability of the results, we collected a total of 25 trials from different initial conditions. We measured the variables $\theta_2^{(1)}$ and $\theta_2^{(2)}$, to which we added zero-mean white Gaussian measurement noise at an intensity of 1% of the signal energy, i.e., 40 dB of signal to noise ratio (SNR).

In the second numerical example, we considered a heterogeneous network composed of three structurally different dynamical subsystems, namely, Rössler (R), Lorenz (L), and Colpitts (C) dynamical systems [36,38,39]. We coupled them corresponding to the three situations reported in Figs. 1(b)–1(d). Indeed, these three coupling schemes are representative of multivariate settings in which spurious relationships can arise when the analysis is limited to a subset of the interacting subsystems [40,41]. In Fig. 1(b), a direct connection between R and C may be inferred when the analysis does not marginalize the knowledge about L. In Fig. 1(c) a direct connection between L and C may be inferred because of the common source R, also called a confounder. In Fig. 1(d), a nonexistent interaction between R and C may be inferred because of their common destination or child L.

The equations governing the dynamics of these three coupled oscillators are

$$\dot{\theta}_1^{(1)} = T[\theta_2^{(1)} + \theta_3^{(1)} + \mathcal{C}^{(1,2)}(\theta_1^{(2)} - \theta_1^{(1)}) + \mathcal{C}^{(1,3)}(\theta_1^{(3)} - \theta_1^{(1)}) + \eta_1^{(1)}],$$

$$\dot{\theta}_2^{(1)} = T(\theta_1^{(1)} + a\theta_2^{(1)} + \eta_2^{(1)}),$$

$$\dot{\theta}_3^{(1)} = T[b + \theta_3^{(1)}(\theta_1^{(1)} - c) + \eta_3^{(1)}],$$

$$\dot{\theta}_1^{(2)} = \sigma(\theta_2^{(2)} - \theta_1^{(2)}) + \mathcal{C}^{(2,1)}(\theta_1^{(1)} - \theta_1^{(2)}) + \mathcal{C}^{(2,3)}(\theta_1^{(3)} - \theta_1^{(2)}) + \eta_1^{(2)},$$

$$\dot{\theta}_2^{(2)} = r\theta_1^{(2)} - \theta_2^{(2)} - \theta_1^{(2)}\theta_3^{(2)} + \eta_2^{(2)},$$

$$\dot{\theta}_3^{(2)} = \theta_1^{(2)}\theta_2^{(2)} - \beta\theta_3^{(2)} + \eta_3^{(2)},$$

$$\dot{\theta}_1^{(3)} = T\left(\frac{g}{Q(1-k)}[\alpha(1-e^{-\theta_2^{(3)}}) + \theta_3^{(3)}] + \mathcal{C}^{(3,1)}(\theta_2^{(1)} - \theta_2^{(3)}) + \mathcal{C}^{(3,2)}(\theta_2^{(2)} - \theta_2^{(3)}) + \eta_1^{(3)}\right),$$

$$\dot{\theta}_2^{(3)} = T\left(\frac{g}{Qk}[(1-\alpha)(1-e^{-\theta_2^{(3)}}) + \theta_3^{(3)}] + \eta_2^{(3)}\right),$$

$$\dot{\theta}_3^{(3)} = -T\left(\frac{Qk(1-k)}{g}(\theta_1^{(3)} + \theta_2^{(3)}) + \frac{1}{Q}\theta_3^{(3)} + \eta_3^{(3)}\right), \quad (12)$$

where $\theta_j^{(1)}, \theta_j^{(2)}, \theta_j^{(3)}$, $j=1,2,3$, are the state variables of the Rössler, Lorenz, and Colpitts dynamical systems, respectively; $a=0.4$, $b=0.4$, $c=5.7$, $\sigma=10$, $\beta=8/3$, $r=28$, $g=10^{0.625}$, $Q=10^{0.15}$, $\alpha=0.996$, and $k=0.5$ are standard valued parameters; $\eta_j^{(i)}$, $i,j=1,2,3$, are zero-mean uncorrelated Gaussian random noises (set to the strength of 1% of the energy of the right-hand side along the uncoupled attractors); and $\mathcal{C}^{(i,j)}$, $j\neq i$, $i,j=1,2,3$, are the strengths of diffusive couplings between the first-state variables $\theta_1^{(1)}$, $\theta_1^{(2)}$, and $\theta_1^{(3)}$. The parameter $T=6$ is introduced in order to adapt the relative speed differences between the three subsystems. To simulate the three schemes of Figs. 1(b)–1(d), we set the values of the coupling strengths as follows: for Fig. 1(b), $\mathcal{C}^{(1,2)}=\mathcal{C}^{(1,3)}=\mathcal{C}^{(2,3)}=\mathcal{C}^{(3,1)}=0$ and $\mathcal{C}^{(2,1)},\mathcal{C}^{(3,2)}$ nonzero and positive; for Fig. 1(c), $\mathcal{C}^{(1,2)}=\mathcal{C}^{(1,3)}=\mathcal{C}^{(2,3)}=\mathcal{C}^{(3,2)}=0$ and $\mathcal{C}^{(2,1)},\mathcal{C}^{(3,1)}$ nonzero and positive; and for Fig. 1(d), $\mathcal{C}^{(1,2)}=\mathcal{C}^{(1,3)}=\mathcal{C}^{(3,2)}=\mathcal{C}^{(3,1)}=0$ and $\mathcal{C}^{(2,1)},\mathcal{C}^{(2,3)}$ nonzero and positive. To guarantee the validity of the hypothesis of weakly interacting oscillators, the active parameters were varied within the interval [0,0.1] or [0,0.3], depending on the case. Once again, these

[2]The down-sampling was performed via linear interpolation of the signals in the time domain by means of the MATLAB function interp1.

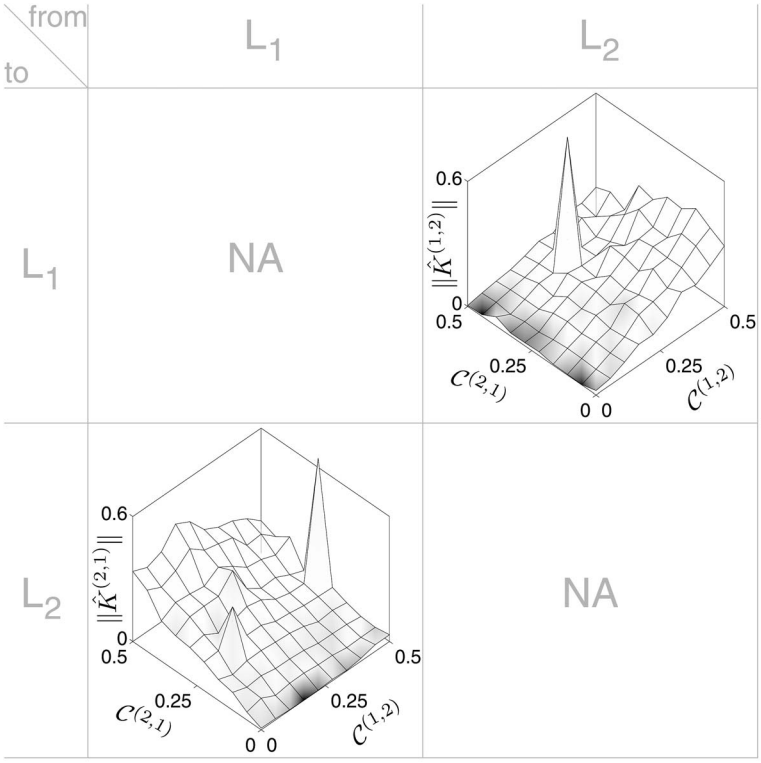

FIG. 2. Method validation: assessment of the ability to discern mutual interdependences; coupling setup as in Fig. 1(a). Dependence of the nontrivial elements of the estimated connectivity matrix $\|\hat{K}^{(i,j)}\|$, $j \neq i$, $i,j=1,2$, upon the mutual coupling parameters $\mathcal{C}^{(1,2)}$ and $\mathcal{C}^{(2,1)}$ of Eq. (11). The surface coloring represents the precision of the estimation, i.e., the ratio of the standard deviation and the mean of the estimated couplings; the whiter the color the higher is the precision.

intervals were chosen such that the synchronization measure introduced in [25] was lower than 0.15 almost everywhere.

Similarly to the previous case, the network was simulated with the Heun method ($\delta t=0.005$) starting every time from random initial conditions, the first 10 000 points of each transient were discarded and, by means of a down-sampling ($\delta T=0.02$), 25 trials of 500 points each were collected. We measured the second-state variables $\theta_2^{(i)}$ from all oscillators, adding zero-mean white Gaussian measurement noise at an intensity of 1% of the signal energy (40 dB SNR).

B. Data analysis setup

By following the three steps described in Sec. II, the analysis of the generated data was performed with the following algorithm. As a first step, the state-space reconstruction from the observations was performed by means of a principal component analysis (PCA) based embedding technique [42]. By following procedures similar to those described in [12,43], we performed the PCA on embedded vectors with unit time delay (i.e., $T_d=0.02$) and 25-step window length (i.e., $T_w=0.5$). Finally, we projected the resulting overembedded space onto the first four components, yielding four-dimensional reconstructed state spaces. This approach is suitable for its robustness to noise and for the orthogonality of the constructed state-space components; the latter is a useful property for the next two steps of (multivariate) identification. We remark that this is related to modern methods that combine features from linear regression and PCA, such as partial least-squares [44], total least-squares [45], and subspace identification techniques [46].

As a second step, radial basis functions (RBFs) were used to fit the self-models and, in order to improve the RBF modeling, we first identified a linear model by ordinary least-squares techniques. RBFs provide a very flexible nonlinear model class and, importantly, an efficient MATLAB toolbox is available [47]. This toolbox has an automatic algorithm for choosing the number of RBFs as well as their centers and radii. In particular, RBF centers and radii are generated by using regression trees, and model selection is performed by considering maximum marginal likelihood.[3]

As a third step, a regularized ordinary least-squares approach was used [48] to identify the cross dependences. We used regularization because of the high number of independent variables (i.e., state-space components) involved in this regression step.

As discussed in Sec. II C, at this point a single number quantifying the influence from $y^{(j)}$ to $y^{(i)}$ would be more suitable than the estimated connectivity matrix $\hat{K}^{(i,j)}$. Instead of applying a norm directly, it would be advisable to zero those elements of the connectivity matrices which may represent spurious dependences. To address this concern, we performed the statistical procedure described in Appendix A.

A MATLAB toolbox implementing the three estimation steps according to the mentioned setup is available [56].

C. Results

The results for the directionality assessment are shown in Fig. 2. The surfaces of the nontrivial elements of the esti-

[3]We stress once again that RBFs are not a universal solution but an easy and convenient one for exemplifying the method; other possibilities could be more appropriate depending upon the real case at hand.

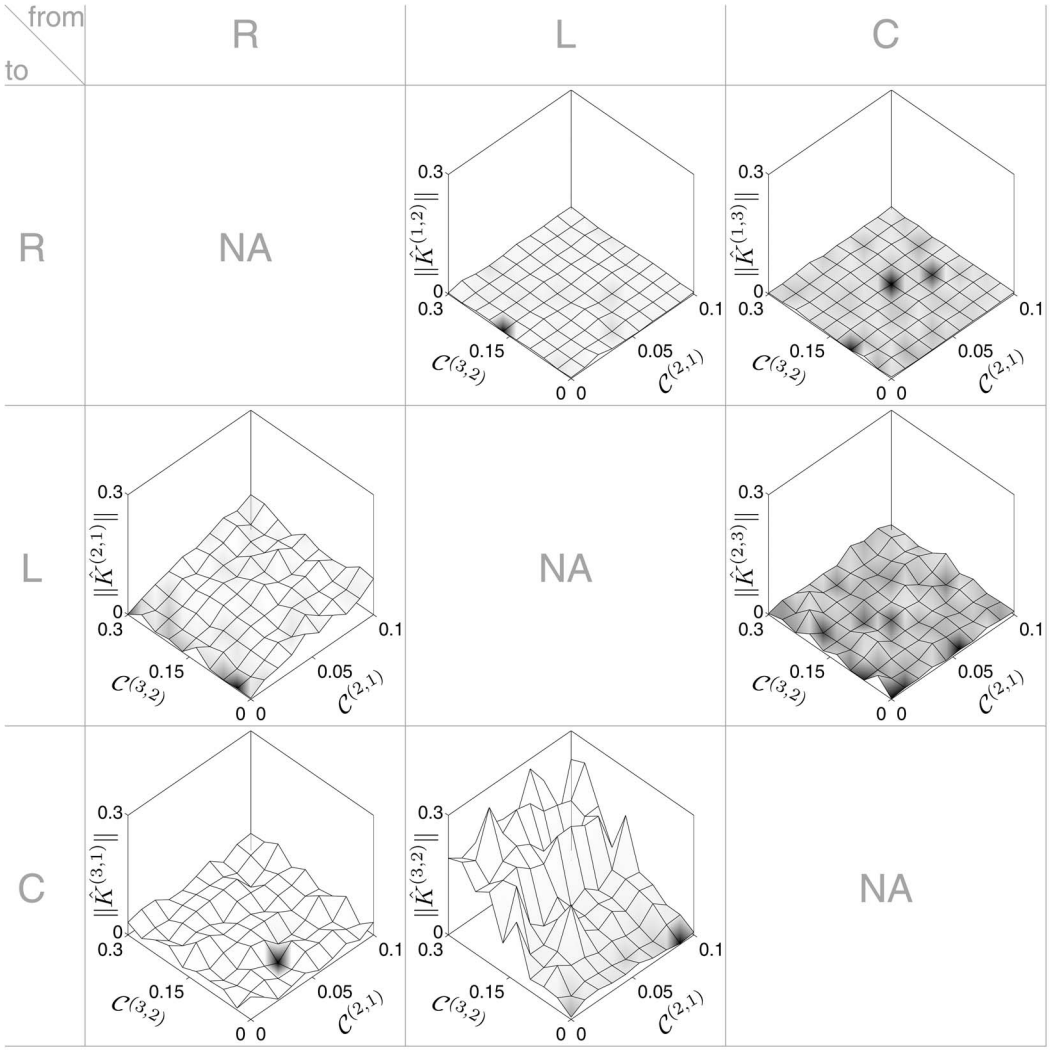

FIG. 3. Method validation: assessment of the ability to discern triangular interdependences in the case of a chain connection; coupling setup as in Fig. 1(b). Dependence of the nontrivial elements of the estimated connectivity matrix $\|\hat{K}^{(i,j)}\|$, $j \neq i$, $i,j=1,2,3$, upon the nonzero mutual coupling parameters $\mathcal{C}^{(2,1)}$ and $\mathcal{C}^{(3,2)}$ of Eq. (12). Surface coloring as in Fig. 2.

mated connectivity matrix $\|\hat{K}^{(i,j)}\|$, $i \neq j$, $i,j=1,2$, are evaluated at 100 evenly spaced points and colored proportionally to the precision of the estimation, i.e., to the ratio of the standard deviation and the mean of the estimated couplings.

The coupling estimates $\|\hat{K}^{(1,2)}\|$ and $\|\hat{K}^{(2,1)}\|$ scale with the mutual coupling strengths $\mathcal{C}^{(1,2)}$ and $\mathcal{C}^{(2,1)}$ [cf. Eq. (11)], respectively, detecting the asymmetry of the mutual influence. We remark that this holds with a few exceptions. These exceptions, for instance at $\mathcal{C}^{(1,2)} \simeq 0.45$ and $\mathcal{C}^{(2,1)} \simeq 0.28$, occur at places where the network undergoes a bifurcation, leading to a jump of 200% (on average over the places) of the synchronization measure previously mentioned [25]. Furthermore, we remark that the estimated couplings decrease slowly with the increase of both coupling strengths. This phenomenon can be explained by the fact that the two subsystems influence each other and, consequently, become more and more similar. However, the directionality and relative strength of the coupling are still correctly estimated and, as testified by the uniform coloring of the surfaces, these estimates are uniformly precise.

The results for the triangular dependency assessment are reported in Figs. 3–5, where the surfaces of the nontrivial elements of the estimated connectivity matrix $\|\hat{K}^{(i,j)}\|$, $i \neq j$, $i,j=1,2,3$, are evaluated again at 100 evenly spaced points and colored proportionally to the precision of the estimation, i.e., to the ratio of the standard deviation and the mean of the estimated couplings.

Figure 3 shows the results relative to the coupling setup of Fig. 1(b). It shows that $\|\hat{K}^{(2,1)}\|$ and $\|\hat{K}^{(3,2)}\|$ scale correctly with their corresponding coupling strengths $\mathcal{C}^{(2,1)}$ and $\mathcal{C}^{(3,2)}$ of Eq. (12), while all the other estimated interdependences do not scale with either of the couplings. In particular, this is remarkable for $\|\hat{K}^{(3,1)}\|$ and $\|\hat{K}^{(1,3)}\|$, which, in a bivariate inference approach, would scale with the couplings.

Figure 4 shows the results relative to the coupling setup of Fig. 1(c). It shows that $\|\hat{K}^{(2,1)}\|$ and $\|\hat{K}^{(3,1)}\|$ scale correctly with their corresponding coupling strengths $\mathcal{C}^{(2,1)}$ and $\mathcal{C}^{(3,1)}$ of Eq. (12). Once again, the other estimated interdependences do not scale with either of the couplings. In particu-

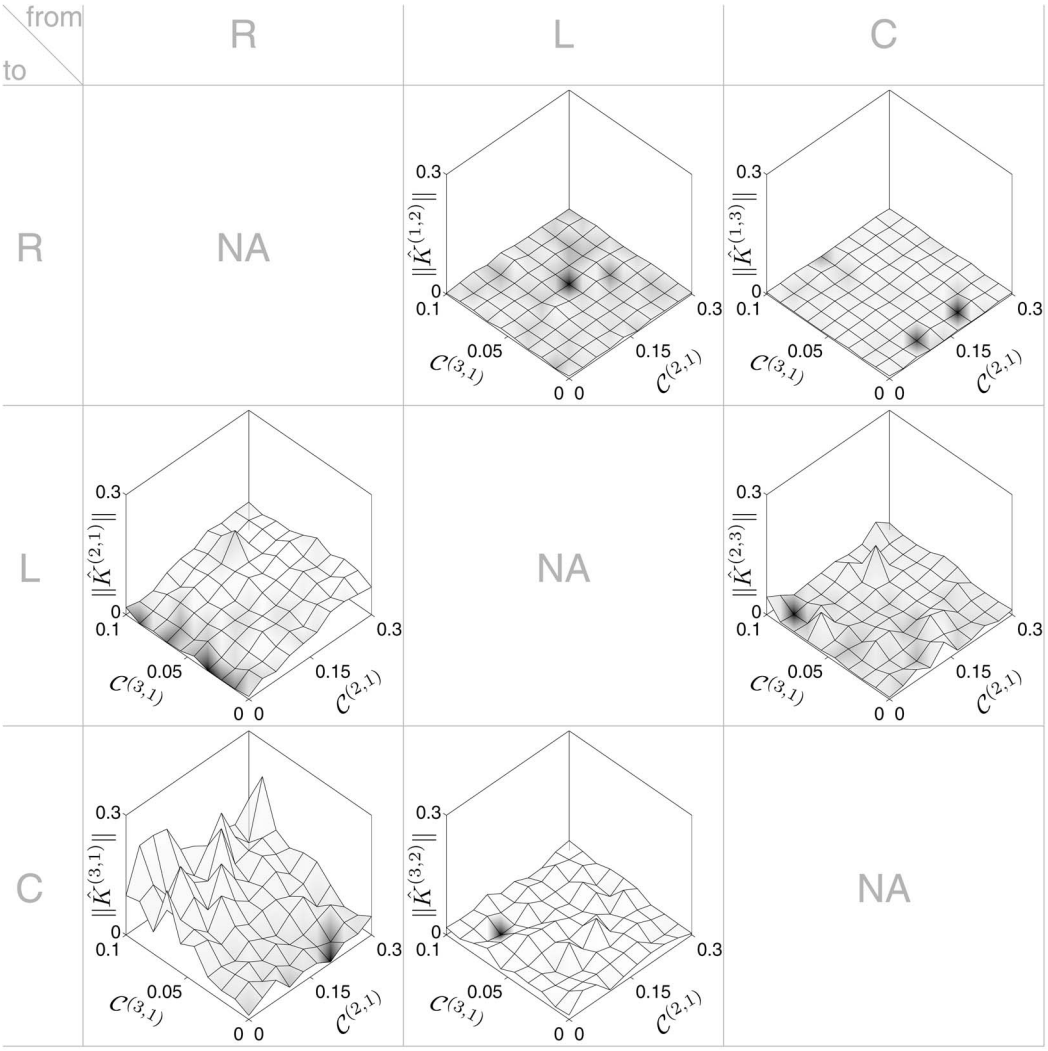

FIG. 4. Method validation: assessment of the ability to discern triangular interdependences in the case of a common source; coupling setup as in Fig. 1(c). Dependence of the nontrivial elements of the estimated connectivity matrix $\|\hat{K}^{(i,j)}\|$, $j \neq i$, $i,j=1,2,3$, upon the nonzero mutual coupling parameters $\mathcal{C}^{(2,1)}$ and $\mathcal{C}^{(3,1)}$ of Eq. (12). Surface coloring as in Fig. 2.

lar, this is true for $\|\hat{K}^{(3,2)}\|$ and $\|\hat{K}^{(2,3)}\|$, which, in a bivariate inference approach, would scale with the couplings.

Similarly, Fig. 5 shows the results relative to the coupling setup of Fig. 1(d). Once again, the estimated active couplings ($\|\hat{K}^{(2,1)}\|$ and $\|\hat{K}^{(2,3)}\|$) scale with their corresponding coupling strengths ($\mathcal{C}^{(2,1)}$ and $\mathcal{C}^{(2,3)}$), and the values of the estimated inactive couplings ($\|\hat{K}^{(1,2)}\|$, $\|\hat{K}^{(1,3)}\|$, $\|\hat{K}^{(3,1)}\|$, and $\|\hat{K}^{(3,2)}\|$) remain close to zero; in particular, $\|\hat{K}^{(3,1)}\|$ and $\|\hat{K}^{(1,3)}\|$, which would turn out to be nonzero in a bivariate analysis setup.

For all three cases, from the rather uniform coloring of the surfaces, we remark that the estimates are uniformly precise.

For most of the cases considered, the graph topology could be correctly inferred, because the inactive estimated couplings are close to zero and lower than the estimated active ones, though there are exceptions, in particular when the active couplings are very low.

Finally, it is worth mentioning that in real applications only one or a pair of conditions might be observed. In this case, it will be necessary to proceed to a statistical assessment of the presence or absence of the estimated couplings in order to extract the graph topology. In general, the details of this assessment will depend on the application at hand and we do not describe any specific recipes here; however, we remark that the use of F tests, exploiting the covariance matrix of the estimates as provided by the least-squares estimation, may notably simplify this step.

IV. ROBUSTNESS ASSESSMENT

In real applications, the signal analyzer commonly has to deal with the problems arising from noise and the small amount of data. The aim of this section is to assess the sensitivity of the method with respect to the amount of data available and to the level of noise. At the same time, the results of the method proposed here are compared with those obtained via phase dynamics modeling [17]. This latter has been chosen as a reference because of its similarity with the method proposed here; in particular, it can be extended to multivariate signals [27] and, similarly to the method pre-

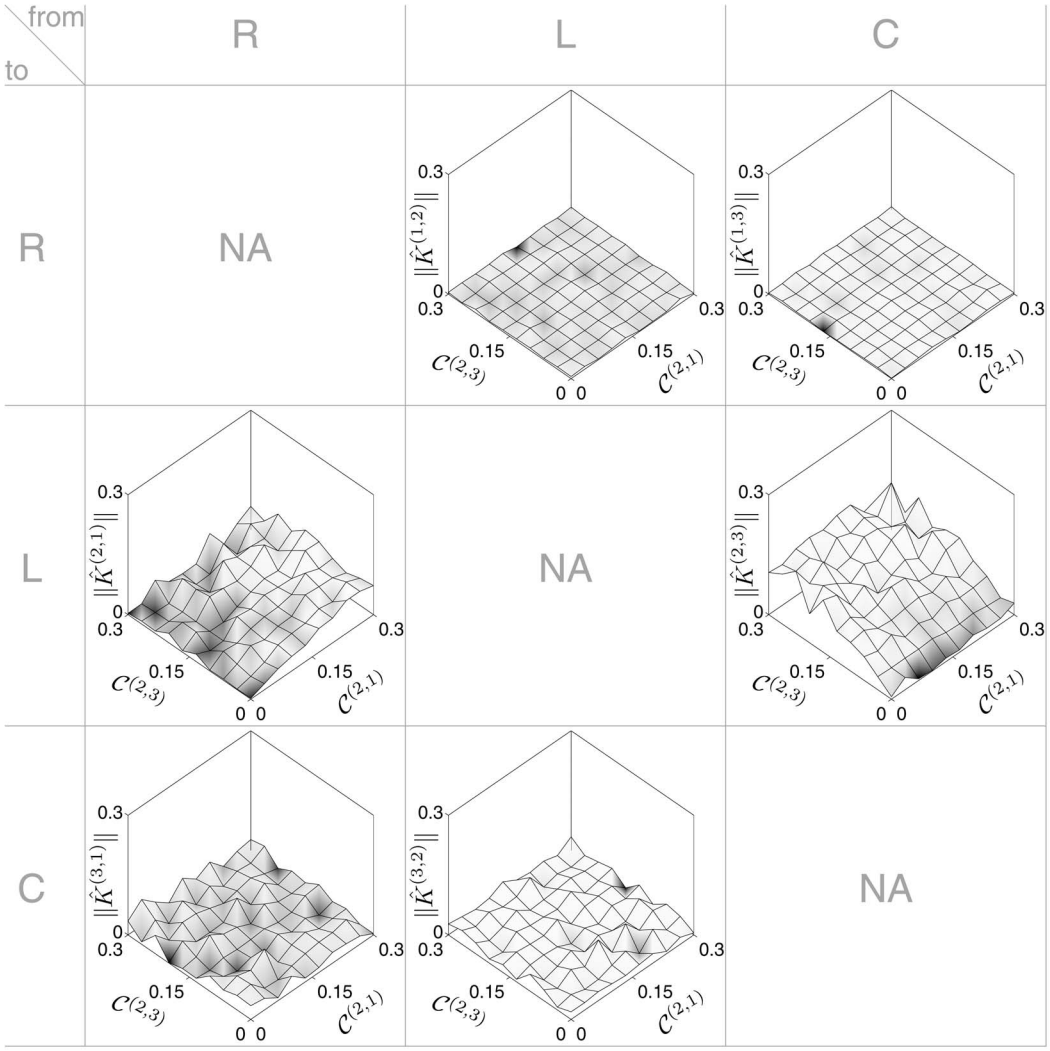

FIG. 5. Method validation: assessment of the ability to discern triangular interdependences in the case of a common child; coupling setup as in Fig. 1(d). Dependence of the nontrivial elements of the estimated connectivity matrix $\|\hat{K}^{(i,j)}\|$, $j \neq i$, $i,j=1,2,3$, upon the nonzero mutual coupling parameters $\mathcal{C}^{(2,1)}$ and $\mathcal{C}^{(2,3)}$ of Eq. (12). Surface coloring as in Fig. 2.

sented here, is conceived for weakly coupled deterministic dynamical systems. For convenience of the reader, the method based on phase dynamics modeling is briefly described in Appendix B.

Although both considered methods can be applied to multivariate signals, to ease the comparison and the interpretation of the results, we have considered a bivariate test bed. More precisely, we considered a unidirectionally coupled network, where an autonomous Rössler oscillator drives a Lorenz oscillator, as shown in Fig. 1(e). Furthermore, in order to deny the two most restricting hypotheses of our modeling, i.e., linear coupling and determinism, we considered nonlinearly coupled subsystems and an increasing amount of modeling noise. The governing equations are

$$\dot{\theta}_1^{(1)} = T(\theta_2^{(1)} + \theta_3^{(1)} + \eta_1^{(1)}),$$

$$\dot{\theta}_2^{(1)} = T(\theta_1^{(1)} + a\theta_2^{(1)} + \eta_2^{(1)}),$$

$$\dot{\theta}_3^{(1)} = T[b + \theta_3^{(1)}(\theta_1^{(1)} - c) + \eta_3^{(1)}],$$

$$\dot{\theta}_1^{(2)} = \sigma(\theta_2^{(2)} - \theta_1^{(2)}) + \mathcal{C}^{(2,1)}(\theta_1^{(1)})^3 + \eta_1^{(2)},$$

$$\dot{\theta}_2^{(2)} = \rho\theta_1^{(2)} - \theta_2^{(2)} - \theta_1^{(2)}\theta_3^{(2)} + \eta_2^{(2)},$$

$$\dot{\theta}_3^{(2)} = \theta_1^{(2)}\theta_2^{(2)} - \beta\theta_3^{(2)} + \eta_3^{(2)}, \tag{13}$$

where $\theta_j^{(1)}$ and $\theta_j^{(2)}$, $j=1,2,3$, are the state variables of the Rössler and Lorenz subsystems, respectively; a, b, c, σ, β, and r are parameters that are fixed at the standard values, i.e., $a=0.4$, $b=0.4$, $c=5.7$, $\sigma=10$, $\beta=8/3$, and $r=28$; the time scale $T=6$ once again adapts the speed of the Rössler to that of the Lorenz system; and, finally, the parameter $\mathcal{C}^{(2,1)}$ is varied in the range $[0,0.03]$ so that we have weak, though nonlinear, coupling between the two subsystems.

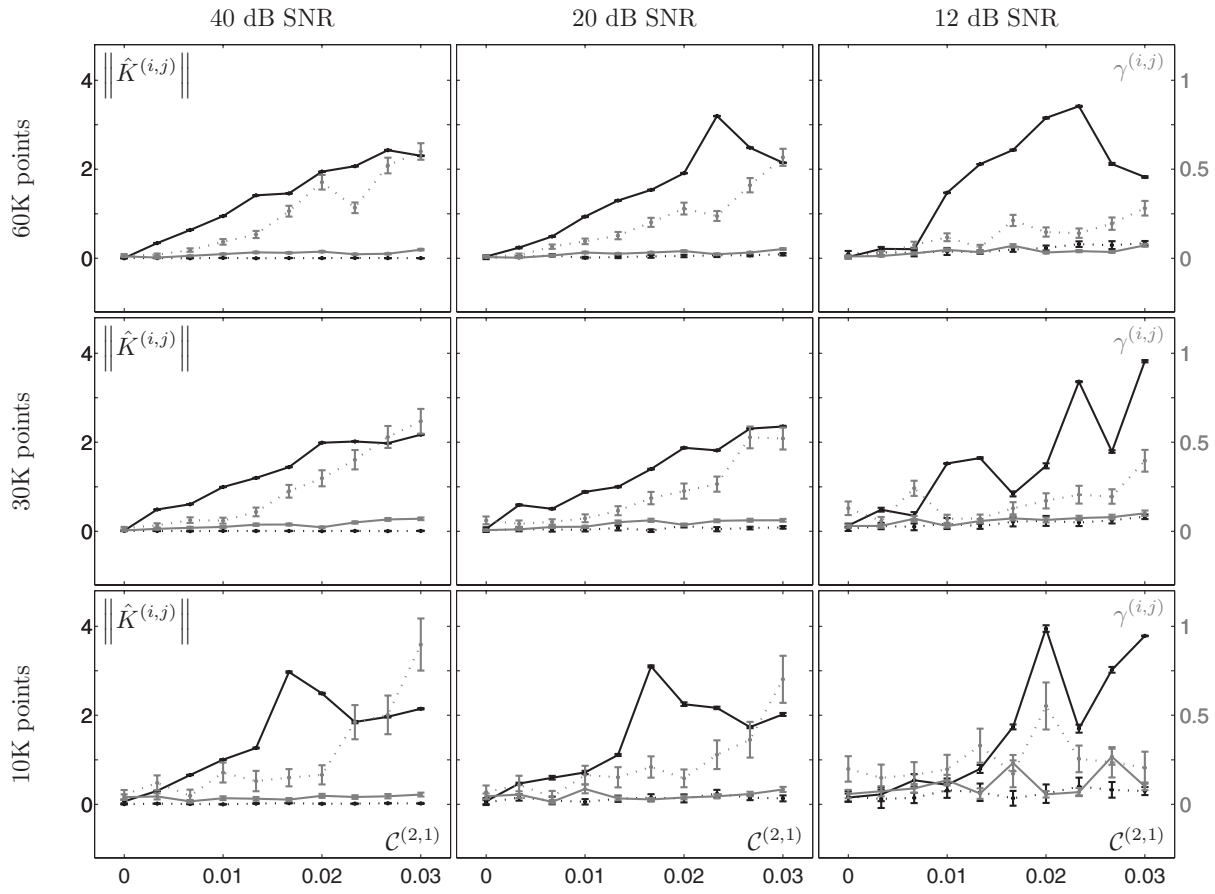

FIG. 6. Method validation: assessment of the robustness with respect to data length (number of thousands of points along the rows) and intensity of measurement noise (SNR along the columns); coupling setup as in Fig. 1(e). Dependence of the estimated coupling between the two subsystems of Eq. (13) upon the nonlinear coupling strength $\mathcal{C}^{(2,1)}$ estimated with two different techniques: the method proposed here (black) and phase dynamics modeling (gray); from subsystem 1 to 2, solid curves; from subsystem 2 to 1, dotted curves. The dots and errors bars illustrate the mean values and standard deviations of the estimations, respectively.

For every considered value of $\mathcal{C}^{(2,1)}$ and modeling noise intensity, the differential equations were iterated, starting from random initial conditions, using the Heun algorithm with $\delta t=0.005$; the initial 10 000 points of each transient were dropped and, by means of a down-sampling ($\delta T=0.02$), we collected a total of 60 000 points, measuring the coupled variables $\theta_1^{(1)}$ and $\theta_1^{(2)}$.

The robustness of the method with respect to measurement and modeling noise and data length was assessed as follows. To assess the sensitiveness with respect to measurement noise intensity, we fixed the modeling noise intensity to 40 dB (SNR) and we considered zero-mean white Gaussian measurement noise at different intensities, i.e., 40, 20, and 12 dB (SNR). For the sensitivity to modeling noise intensity, we fixed the measurement noise intensity to 40 dB (SNR) and we considered white Gaussian modeling noise at different intensities, i.e., 36, 20, and 12 dB (SNR). Afterward, for each of the considered values of $\mathcal{C}^{(2,1)}$ and measurement and modeling noise intensities, the two measures of interdependence were computed by considering 10 000, 30 000 or all 60 000 data points.

For the method presented here, we used the same settings as described in Sec. III B, while for the phase dynamics based method we used the Hilbert transform[4] to compute instantaneous phases from the time series $\tau=0.3$, and a third-order Fourier expansion[5] for estimating the F in Eq. (B1).

A. Results

The results are summarized in Figs. 6 and 7, which compare the dependence of the four estimated interdependences $\|\hat{K}^{(2,1)}\|$, $\|\hat{K}^{(1,2)}\|$, $\gamma^{(2,1)}$, and $\gamma^{(1,2)}$ upon the coupling parameter $\mathcal{C}^{(2,1)}$ of Eq. (13) at different noise intensities and number of points considered. Black curves denote $\|\hat{K}^{(i,j)}\|$ and gray

[4]Although the analytic approach given by the Hilbert transform provides a unique determination of the phase of a signal, it cannot avoid the ambiguity of defining the phase for a dynamical system since the result depends on the choice of the observable. *A priori*, in a blind experimental setup, one has no control on the choice of the observable; hence, we estimated the phase via Hilbert transform because it is the most commonly used in experimental studies. However, it is worth mentioning that very recently a technique potentially encompassing this issue was proposed in [55].

[5]We mention the fact that the order of the Fourier expansion may influence the results to some extent.

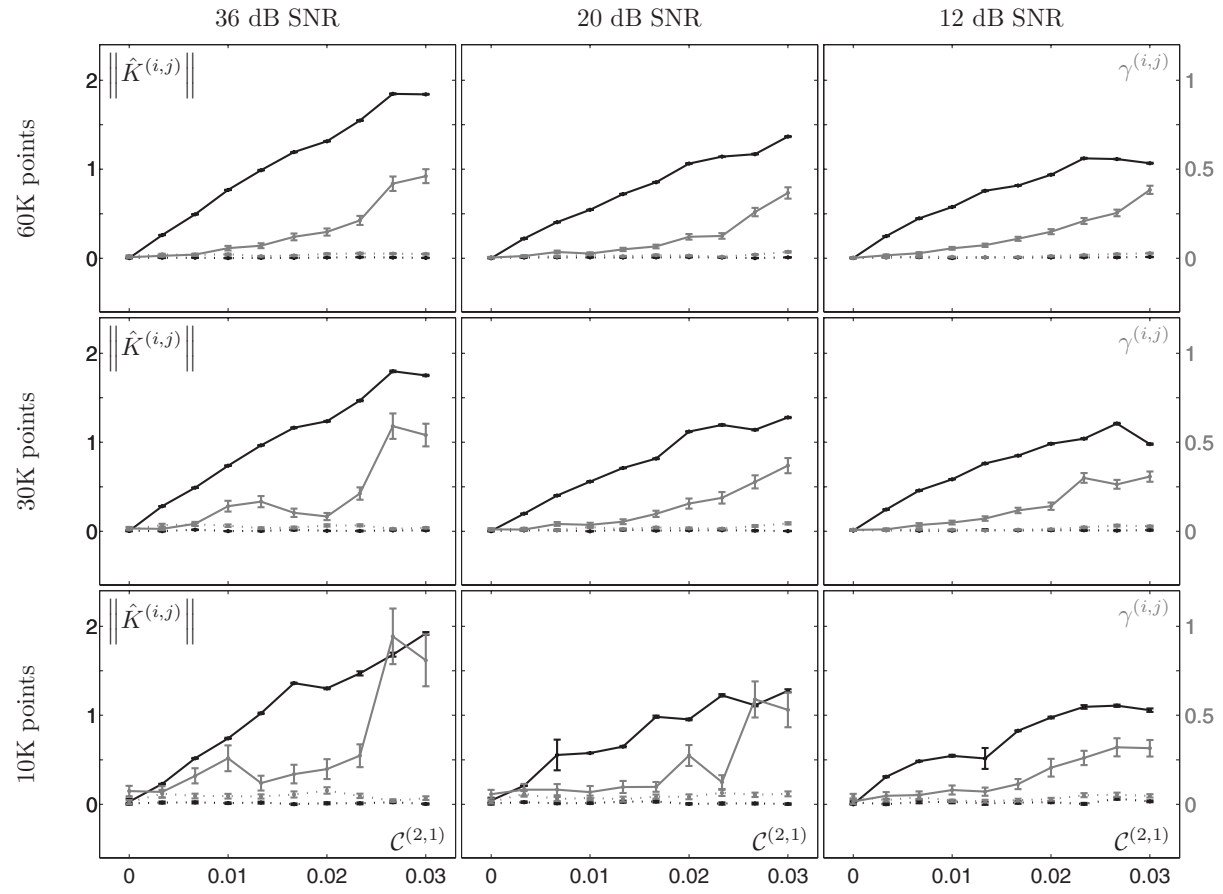

FIG. 7. Method validation: assessment of the robustness with respect to data length (number of thousands of points along the rows) and intensity of modeling noise (SNR along the columns); coupling setup as in Fig. 1(e). Dependence of the estimated coupling between the two subsystems of Eq. (13) upon the nonlinear coupling strength $\mathcal{C}^{(2,1)}$ estimated with two different techniques: method proposed here (black) and phase dynamics modeling (gray); from subsystem 1 to 2, solid curves; from subsystem 2 to 1, dotted curves. The dots and errors bars illustrate the mean values and standard deviations of the estimations, respectively.

curves are for $\gamma^{(i,j)}$; the solid curves denote the estimated active coupling, i.e., from the Rössler to the Lorenz subsystem, and the dotted curves denote the estimated inactive coupling, i.e., from the Lorenz to the Rössler subsystem.

For most cases, the estimated active coupling, i.e., $\|\hat{K}^{(2,1)}\|$ and $\gamma^{(2,1)}$, are consistently bigger than the estimated inactive ones, i.e., $\|\hat{K}^{(1,2)}\|$ and $\gamma^{(1,2)}$, which indeed remain close to zero. Consequently, for most, though not all, of the considered coupling strengths, both methods would allow the inference of the correct topology and directionality of the couplings.

As expected, for both methods the estimated interdependences worsen with higher noise intensity and/or small data length. The method presented here appears to be less sensitive to measurement noise, though for both methods a threshold phenomenon take place in the detection of the active coupling; this phenomenon is more marked the fewer the data points. Concerning the sensitiveness with respect to the modeling noise, when enough data are available both methods perform well even when the hypothesis of determinism is severely affected, i.e., in the presence of strong modeling noise (12 dB SNR). However, the modeling noise seems to affect more the method based on the phase dynamics than the method presented here.

In general, for this numerical setup for which a phase can be defined, the interdependence estimated with the method presented here is consistent with the interdependence estimated via the phase dynamics. However, on average, the former appears to be more reliable (see the error bars), less sensitive to both measurement and modeling noise, and could be applied to arbitrary signals, even when a phase cannot be defined.

Finally, it is worth mentioning that similar results were obtained when observing the noncoupled state variables and/or considering a quadratic coupling.

V. SCALABILITY

Hitherto, we have tested the capability of the method in standard problems arising in multivariate settings. Still, we shall discuss its computational feasibility when dealing with generic P-variate measurements.

Within our gray-box modeling framework, as reported in the procedure described in Sec. II, we first estimate P "self-models," and then we estimate the cross dependences by means of a multiple linear regression. Consequently, the costly nonlinear identification part is done separately on each

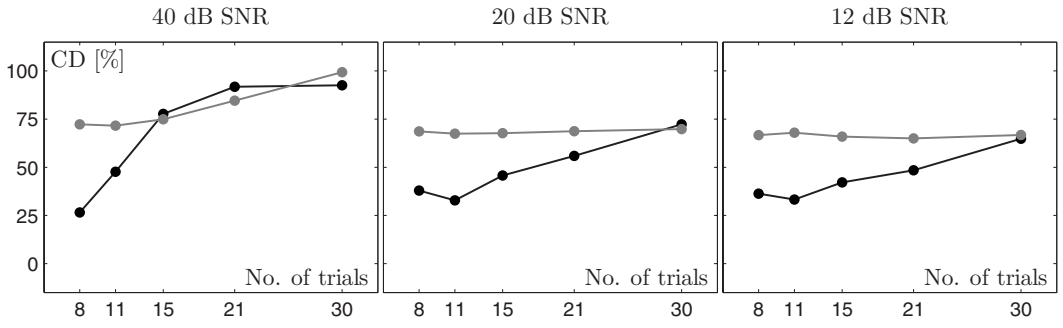

FIG. 8. Method validation: assessment of the scalability to large numbers of dynamical systems; setup: 128 coupled nonidentical Colpitts dynamical systems [cf. Eq. (14)]. Dependence of the percentage of correctly detected couplings upon data length (number of trials of 1000 samples each) and intensity of measurement noise (SNR): percentage of correctly detected present (black) and absent (gray) couplings.

of the P subsystems, potentially over a few variables at a time. Only the final linear regression is done over all the variables; for the linear regression we can take advantage of existing efficient software packages [49] which can consider millions of variables in reasonable time.

In this section, we describe a test performed to assess the effectiveness of the method when dealing with a large number of observed subsystems. In particular, we have chosen $P=128$, because it represents the state of the art in modern experimental setups [25,50,51]. We considered a network of linearly coupled nonidentical Colpitts oscillators, namely,

$$\dot{\theta}_1^{(i)} = \frac{g^{(i)}}{Q^{(i)}(1-k)}[\alpha(1-e^{-\theta_2^{(3)}}) + \theta_3^{(i)}] + \sum_{j\neq i} \mathcal{C}^{(i,j)}(\theta_1^{(j)} - \theta_1^{(i)}) + \eta_1^{(i)},$$

$$\dot{\theta}_2^{(i)} = \frac{g^{(i)}}{Q^{(i)}k}[(1-\alpha)(1-e^{-\theta_2^{(3)}}) + \theta_3^{(i)}] + \eta_2^{(i)},$$

$$\dot{\theta}_3^{(i)} = -\frac{Q^{(i)}k(1-k)}{g^{(i)}}(\theta_1^{(i)} + \theta_2^{(i)}) - \frac{1}{Q^{(i)}}\theta_3^{(i)} + \eta_3^{(i)}, \quad (14)$$

where $\theta_j^{(i)}$, $j=1,2,3$, are the state variables of each subsystem $i=1,\ldots,128$; α and k are parameters fixed at the standard values 0.996 and 0.5; $Q^{(i)}$ and $g^{(i)}$ are parameters whose values are chosen randomly in an interval ($\pm 10\%$) around the standard values $10^{0.15}$ and $10^{0.625}$, respectively; $\eta_j^{(i)}$ are zero-mean uncorrelated Gaussian random noises (set in simulations to a variance of 1% of the energy of the right-hand side along the uncoupled attractors); and $\mathcal{C}^{(i,j)}$ are the strengths of diffusive couplings between the first-state variables. We randomly set the connectivity within the network by choosing an average of two couplings for each subsystem, with a strength value of 0.07 to satisfy the hypothesis of weakly interacting oscillators.

The differential equations were iterated, starting from random initial conditions, using the Heun algorithm with $\delta t = 0.025$, the initial 10 000 points of each transient were dropped and, by means of a down-sampling ($\delta T = 0.063$), time series of length $L=1000$ were recorded. We collected a total of 30 trials from different initial conditions, measuring the second state variable of each subsystem, i.e., $\theta_2^{(i)}, i = 1,\ldots,128$, to which we added zero-mean white Gaussian measurement noise of different intensities, i.e., 40, 20, and 12 dB (SNR). Afterward, we assessed the robustness of the method with respect to measurement noise and data length. This was done for the chosen connectivity matrix and measurement noise intensities, over 5, 8, 12, 20, and all the 30 trials.

A. Results

The results are reported in Fig. 8, which shows the dependence of the percentage of correctly detected couplings upon the number of available data points at the different noise intensities considered. That is, by partitioning all the estimated interdependences $\|\hat{K}^{(i,j)}\|$ into two clusters, we labeled the couplings as either present or absent. Figure 8 reports the percentage of the correctly detected nonzero and zero couplings (black and gray curves, respectively).

In general, we expect the percentage of the correctly detected absent couplings to be higher than that of the present couplings, simply because in the considered setup there are 16 000 zero connections against 256 nonzero connections.

The result shows that the reliability of coupling detection is very high for small noise intensities and, generally, increases with the amount of data available and decreases with the measurement noise intensity. However, in the case of strong noise intensity (i.e., 12 dB of SNR), the percentage of good detections does not fall below 60% when an adequate number of points is considered. Note that the power of the method, i.e., the percentage of good detections, is remarkably higher than a purely combinatorial guess, which would already results in percentages as low as 2% if we knew exactly the number of active links.

VI. DISCUSSION AND CONCLUSIONS

We have proposed a computationally viable method to infer from multivariate time series the connectivity matrix of a network of weakly interacting dynamical systems. In common with other approaches, the method exploits dynamical properties of the data, and we focused on the problem of inferring weak couplings also because they are important in applications [52,53].

Being intrinsically multivariate and computationally viable, the method is particularly suitable for modern experimental setups, where it is increasingly common to record, separately but in parallel, the dynamical activity of several components of the systems under observation.

The intrinsic computational viability is structurally given by the arrangement of the method into three sequential operations, i.e., a series of state-space reconstructions, a series of nonlinear regressions, and one linear regression. Of these operations, the costly nonlinear regression is done iteratively on few variables at a time, and only the linear regression is performed over all the variables. Moreover, many well-established techniques are available for performing these three operations; hence, each one of them can be independently tuned to the specific application without severely affecting the computational complexity of the whole estimation.

Concerning the linear regression, it is worth stressing that the use of (ordinary) least-squares methods allows the estimation of the couplings together with their covariance matrix. If Gaussian assumptions are tenable, that makes easy the use of F tests for the statistical assessment of the results. This has a twofold consequence: first, the statistical analysis of the (linear) connectivity model can be performed without time-consuming techniques such as bootstrapping; second, if needed, it is possible to compute the power of multiple null hypotheses against selected alternative hypotheses of interest.

When tested on numerically generated data, the method proved to be able to infer: the asymmetry of coupling for two mutually coupled nonidentical systems; and the graph topology of three coupled heterogeneous systems in three typical setups where bivariate methods would fail. It proved also to work in the case of nonlinearly coupled systems with strong modeling noise, a case that severely violates the two most restrictive modeling hypotheses, i.e., linear coupling and determinism. Moreover, when compared with a method based on phase dynamics modeling, the two methods gave consistent results. Concerning this last point, we remark that, while the proposed method has the advantage of not requiring the extraction of the phases, which makes it applicable to a wider class of signals, this may have the disadvantage of being more prone to errors because it takes into account the whole dynamics of the network.

Finally, it is important to stress that the proposed method does not constitute a panacea. In fact, it relies on several hypotheses, not the least the assumption that we measure at least one time series from each of the subsystems in the network. However, among the modern demands of multivariate data analysis, it shows as a promising deterministic modeling based approach, and joins the community of techniques which the expert signal analyzers should all take into account when facing real data.

To conclude, we would like to mention the possibility of relaxing the weak-coupling hypothesis. Despite being theoretically possible from the (numerical) modeling point of view, it raises the nontrivial problem of the network's state-space reconstruction from multivariate data, an interesting problem, whose discussion, however, goes beyond the scope of this paper.

ACKNOWLEDGMENTS

The authors thank M. Hasler for useful discussions. This work was supported by the European Project BRACCIA (Grant No. NEST-517133).

APPENDIX A: ASSESSING STATISTICALLY SIGNIFICANT DEPENDENCES

Here, we report the procedure used to estimate the influence of a subsystem (j) on a subsystem (i) starting from the connectivity matrix $\hat{K}^{(i,j)}$ identified in Sec. II C. For the sake of simplicity, let us focus on a generic element of $\hat{K}^{(i,j)}$, which, to simplify the notation, we denote simply as $\hat{k}$.

Thanks to the least-squares procedure, we also have an estimate of its standard deviation, which we denote $\hat{\sigma}$. Under the assumption that $\hat{k}$ is normally distributed, with mean μ and variance σ^2, we wish to test the null hypothesis

$$H_0: \ \mu = 0, \sigma = \hat{\sigma},$$

against the alternative hypothesis

$$H_1: \ \mu = \hat{k}, \sigma = \hat{\sigma}.$$

From F statistics, we can easily compute the p value; namely, the probability of a *type-I error*, which is the probability that we may wrongly reject the null hypothesis H_0 when it is true. Afterward, the p value can be used to compute the probability β that we may wrongly accept H_0 when it is false, i.e., the probability of a *type-II error*. Usually, its complementary probability, i.e., $1-\beta$, is called the *power* of the test of the hypothesis H_0 against the alternative hypothesis H_1 [34]. Under the normal distribution hypothesis, the power is given by

$$1 - \beta = G\{\sqrt{L'}\hat{k}/\hat{\sigma} - z\}, \tag{A1}$$

where L' is the number of samples used to get the estimate $\hat{k}$, G is the standardized normal distribution function, and z is such that $G(-z)=p$ holds. We fixed the power of our hypothesis testing to $1-\beta=0.95$, i.e., we allowed 5% of type-II errors, and, consequently, we zeroed $\hat{k}$ if the power computed in Eq. (A1) exceeded this value.

Finally, after repeating the same procedure for all the elements of $\hat{K}^{(i,j)}$, we applied a two-norm to obtain an estimate of the influence of subsystem (j) on (i).

APPENDIX B: ESTIMATION OF INTERACTIONS VIA PHASE DYNAMICS MODELING

Here, we briefly describe the method, initially proposed in [17], for estimating the influence of a subsystem (j) on a subsystem (i) via phase dynamics modeling. Similarly to the method proposed here, this method assumes measurement of one time series from each of the subsystems in the network. Afterward, once the instantaneous phases have been estimated from the measured signals, this method tests whether the future time evolution of the phase of one oscillator is influenced by the phase of the other oscillators.

To keep the description simple, let us consider the case of two oscillators, and let us denote by $\phi_t^{(1)}$ and $\phi_t^{(2)}$ the instantaneous phases estimated from the two signals measured from them. In the first place, the phase increments over a finite time interval τ are computed, i.e., $\Delta_t^{(i)}=\phi_{t+\tau}^{(i)}-\phi_t^{(i)}$, $i=1,2$. Afterward, these increments are considered as being generated by some unknown noisy map

$$\Delta_t^{(i)} = F^{(i)}(\phi_t^{(1)}, \phi_t^{(2)}) + \xi_t^{(i)}, \quad i = 1,2, \tag{B1}$$

and, by using a finite Fourier series, a least-squares estimate of this map, we call it $\hat{F}^{(i)}$, is obtained. Finally, the interdependence of the phase dynamics from subsystem 2 to subsystem 1 is quantified by means of the following coefficient:

$$\gamma^{(1,2)} = \int_0^{2\pi} \int_0^{2\pi} \left(\frac{\partial \hat{F}^{(1)}}{\partial \phi^{(2)}} \right)^2 d\phi^{(1)} d\phi^{(2)}. \tag{B2}$$

Clearly, the interdependence in the other direction, i.e., $\gamma^{(2,1)}$, can be computed in a similar way.

Finally, it is worth noticing that the lack of bias of the coupling coefficients and the estimation of their variance has been presented in [54].

[1] E. Wilson, *Consilience* (Knopf, New York, 1998).
[2] U. Bhalla and R. Iyengar, Science **283**, 381 (1999).
[3] M. Faloutsos, P. Faloutsos, and C. Faloutsos, Comput. Commun. Rev. **29**, 251 (1999).
[4] R. Williams and N. Martinez, Nature (London) **404**, 455 (2000).
[5] M. Newman, Proc. Natl. Acad. Sci. U.S.A. **98**, 404 (2001).
[6] B. Blasius, A. Huppert, and L. Stone, Nature (London) **399**, 354 (1999).
[7] C. Gray, P. König, A. Engel, and W. Singer, Nature (London) **338**, 334 (1989).
[8] O. Sporns, G. Tononi, and G. Edelman, Cereb. Cortex **10**, 127 (2000).
[9] S. Strogatz, Nature (London) **410**, 268 (2001).
[10] A. Pikovsky, M. Rosenblum, and J. Kurths, *Synchronization, A Universal Concept in Nonlinear Sciences* (Cambridge University Press, Cambridge, U.K., 2001).
[11] R. Quian Quiroga, A. Kraskov, T. Kreuz, and P. Grassberger, Phys. Rev. E **65**, 041903 (2002).
[12] H. Kantz and T. Schreiber, *Nonlinear Time Series Analysis*, 2nd ed. (Cambridge University Press, Cambridge, U.K., 2004).
[13] R. Quian Quiroga, J. Arnhold, and P. Grassberger, Phys. Rev. E **61**, 5142 (2000).
[14] T. Schreiber, Phys. Rev. Lett. **85**, 461 (2000).
[15] M. Wiesenfeldt, U. Parlitz, and W. Lauterborn, Int. J. Bifurcation Chaos Appl. Sci. Eng. **11**, 2217 (2001).
[16] I. Tokuda, J. Kurths, and E. Rosa, Phys. Rev. Lett. **88**, 014101 (2001).
[17] M. Rosenblum and A. Pikovsky, Phys. Rev. E **64**, 045202(R) (2001).
[18] M. Paluš and A. Stefanovska, Phys. Rev. E **67**, 055201(R) (2003).
[19] J. Wittaker, *Graphical Models in Applied Multivariate Statistics* (John Wiley, Chichester, U.K., 1990).
[20] M. Kamiński and K. Blinowska, Biol. Cybern. **65**, 203 (1991).
[21] L. Baccalà and K. Sameshima, Biol. Cybern. **84**, 463 (2001).
[22] R. Dahlhaus, Metrika **51**, 157 (2000).
[23] M. Eichler, R. Dahlhaus, and J. Sandkühler, Biol. Cybern. **89**, 289 (2003).
[24] S. Boccaletti, J. Kurths, G. Osipov, D. Valladares, and C. Zhou, Phys. Rep. **366**, 1 (2002).
[25] C. Carmeli, M. Knyazeva, G. M. Innocenti, and O. De Feo, Neuroimage **25**, 339 (2005).
[26] Y. Chen, G. Rangarajan, J. Feng, and M. Ding, Phys. Lett. A **324**, 26 (2004).
[27] L. Cimponeriu, M. Rosenblum, T. Fieseler, J. Dammers, M. Schiek, M. Majtanik, P. Morosan, A. Bezerianos, and P. Tass, Prog. Theor. Phys. **150**, 22 (2003).
[28] B. Schelter, M. Winterhalder, R. Dahlhaus, J. Kurths, and J. Timmer, Phys. Rev. Lett. **96**, 208103 (2006).
[29] S. Frenzel and B. Pompe, Phys. Rev. Lett. **99**, 204101 (2007).
[30] T. Cover and J. Thomas, *Elements of Information Theory* (John Wiley and Sons, New York, 1991).
[31] L. Paninski, J. Pillow, and E. Simoncelli, Neural Comput. **16**, 2533 (2004).
[32] V. Makarov, F. Panetsos, and O. De Feo, J. Neurosci. Methods **144**, 265 (2005).
[33] T. Sauer, J. Yorke, and M. Casdagli, J. Stat. Phys. **65**, 579 (1991).
[34] A. Stuart, J. Ord, and S. Arnold, *Kendall's Advanced Theory of Statistics, Volume 2A: Classical Inference and the Linear Model*, 6th ed. (Arnold, London, 1999).
[35] J. Higgins, *Introduction to Modern Nonparametric Statistics* (Brooks/Cole-Thomson Learning, Pacific Grove, CA, 2004).
[36] E. Lorenz, J. Atmos. Sci. **20**, 130 (1963).
[37] A. Quarteroni, R. Sacco, and F. Saleri, *Numerical Mathematics* (Springer-Verlag, Berlin, 2004).
[38] O. Rössler, Z. Naturforsch. A **31**, 259 (1976).
[39] O. De Feo, G. M. Maggio, and M. P. Kennedy, Int. J. Bifurcation Chaos Appl. Sci. Eng. **10**, 935 (2000).
[40] C. Hsiao, J. Econ. Dyn. Control **4**, 243 (1982).
[41] R. Dahlhaus, M. Eichler, and J. Sandkühler, J. Neurosci. Methods **77**, 93 (1997).
[42] D. Broomhead and G. King, Physica D **20**, 217 (1986).
[43] M. Small and C. Tse, Physica D **194**, 283 (2004).
[44] I. Hellan, Scand. J. Stat. **17**, 97 (1990).
[45] J. Crassidis and J. Junkins, *Optimal Estimation of Dynamical Systems* (Chapman & Hall/CRC, New York, 2004).
[46] P. Van Overschee and B. DeMoor, *Subspace Identification of Linear Systems: Theory, Implementation, Applications* (Kluwer Academic Publishers, Dordrecht, 1996).
[47] M. Orr, http://www.anc.ed.ac.uk/~mjo/software/rbf2.zip
[48] G. Golub and U. von Matt, Stanford University Technical Report, 1997 (unpublished).
[49] E. Anderson *et al.*, *LAPACK Users' Guide* (Society for Industrial and Applied Mathematics, Philadelphia, 1992).

[50] J. Evans, *Biomolecular NMR Spectroscopy* (Oxford University Press, Oxford, 1996).
[51] D. Santucci, J. Kralik, M. Lebedev, and M. Nicolelis, Eur. J. Neurosci. **22**(6), 1529 (2005).
[52] Y. Kuramoto, *Chemical Oscillations, Waves and Turbulence* (Springer, Berlin, 1984).
[53] K. Likharev, *Dynamics of Josephson Junctions and Circuits* (Gordon and Breach, Philadelphia, 1991).
[54] D. A. Smirnov and B. P. Bezruchko, Phys. Rev. E **68**, 046209 (2003).
[55] B. Kralemann, L. Cimponeriu, M. Rosenblum, A. Pikovsky, and R. Mrowka, Phys. Rev. E **76**, 055201(R) (2007).
[56] http://aperest.epfl.ch/docs/software.htm